Title

The HydG Enzyme Generates an Fe(CO)2(CN) Synthon in Assembly of the FeFe Hydrogenase H-Cluster

Journal

Science, 343(6169)

ISSN

0036-8075

Authors

Kuchenreuther, Jon M
Myers, William K
Suess, Daniel LM
et al.

Publication Date

2014-01-24

DOI

10.1126/science.1246572

Peer reviewed

HHS Public Access

Author manuscript

Science. Author manuscript; available in PMC 2015 July 24.

Published in final edited form as:

Science. 2014 January 24; 343(6169): 424–427. doi:10.1126/science.1246572.

The HydG Enzyme Generates an $Fe(CO)_2(CN)$ Synthon in Assembly of the FeFe Hydrogenase H-Cluster

Jon M. Kuchenreuther[1,*], **William K. Myer**[1,*], **Daniel L. M. Suess**[1], **Troy A. Stich**[1], **Vladimir Pelmenschikov**[2], **Stacey A. Shiigi**[3], **Stephen P. Cramer**[1,4], **James R. Swartz**[3,5], **R. David Britt**[1,†], and **Simon J. George**[1,†]

[1]Department of Chemistry, University of California, Davis, Davis, CA 95616, USA

[2]Institut für Chemie, Technische Universität Berlin, Berlin 10623, Germany

[3]Department of Bioengineering, Stanford University, Stanford, CA 94305, USA

[4]Physical Biosciences Division, Lawrence Berkeley National Laboratory, Berkeley, CA 94720, USA

[5]Department of Chemical Engineering, Stanford University, Stanford, CA 94305, USA

Abstract

Three iron-sulfur proteins–HydE, HydF, and HydG–play a key role in the synthesis of the $[2Fe]_H$ component of the catalytic H-cluster of FeFe hydrogenase. The radical *S*-adenosyl-L-methionine enzyme HydG lyses free tyrosine to produce *p*-cresol and the CO and CN^- ligands of the $[2Fe]_H$ cluster. Here, we applied stopped-flow Fourier transform infrared and electron-nuclear double resonance spectroscopies to probe the formation of HydG-bound Fe-containing species bearing CO and CN^- ligands with spectroscopic signatures that evolve on the 1- to 1000-second time scale. Through study of the ^{13}C, ^{15}N, and ^{57}Fe isotopologs of these intermediates and products, we identify the final HydG-bound species as an organometallic $Fe(CO)_2(CN)$ synthon that is ultimately transferred to apohydrogenase to form the $[2Fe]_H$ component of the H-cluster.

FeFe hydrogenase enzymes rapidly evolve H_2 at a 6-Fe catalytic site termed the H-cluster (Fig. 1A) (1–3), which comprises a traditional 4Fe-4S subcluster ($[4Fe\text{-}4S]_H$), produced by canonical Fe-S cluster biosynthesis proteins, that is linked via a cysteine bridge to a dinuclear Fe subcluster ($[2Fe]_H$) that contains unusual ligands. Specifically, the $[2Fe]_H$ subcluster possesses two terminal CN^- ligands, two terminal CO ligands, and azadithiolate and CO bridges, all of which are thought to be synthesized and installed by a set of Fe-S proteins denoted HydE, HydF, and HydG. In one recent model for the $[2Fe]_H$ center bioassembly pathway (4, 5), the two radical *S*-adenosyl-L-methionine (SAM) enzymes of the

†Corresponding author. rdbritt@ucdavis.edu (R.D.B.); sjgeorge@ucdavis.edu (S.J.G.).
*These authors contributed equally to this work.

Supplementary Materials

www.sciencemag.org/content/343/6169/[page]/suppl/DC1

Materials and Methods
Figs. S1 to S10
Tables S1 and S2
References (27–43)

set, HydE and HydG, generate the dithiolate moiety and free CO and CN^-, respectively, and these ligands are then transferred to a dinuclear Fe precursor bound to HydF, which acts as a scaffold protein for assembling the final $[2Fe]_H$ subunit. Individually expressed HydE, HydF, and HydG can be combined for successful in vitro synthesis of the $[2Fe]_H$ component of the H-cluster and concurrent activation of FeFe hydrogenase apoprotein (6, 7). Alternatively, an abiotically synthesized dinuclear Fe subcluster, constructed with an azadithiolate bridge as well as one CN^- and two CO ligands per Fe, can also be used to activate FeFe hydrogenase (8, 9).

The HydG radical SAM enzyme was previously reported to use free L-tyrosine (Tyr) as its substrate to generate *p*-cresol and free CO and CN^- as its products (6, 10–12). Although HydG has yet to be crystallographically characterized, sequence analysis and results from spectroscopic studies indicate that it has two 4Fe-4S clusters, each with distinct functions (13, 14). The SAM-binding 4Fe-4S cluster, located near the N terminus, reductively cleaves SAM, producing methionine plus a strongly oxidizing 5′-deoxyadenosyl radical (5′-dA•) (15, 16). The second Fe-S cluster, located near the C terminus, was implicated as the site of Tyr binding in our recent investigation of the HydG reaction mechanism using electron paramagnetic resonance (EPR) spectroscopy (17). Also on the basis of EPR spectroscopic results, we proposed that the initial 5′-dA• generates a neutral tyrosine radical bound to this C-terminal 4Fe-4S cluster, which then undergoes heterolytic cleavage at the C_α-C_β bond, forming a 4-oxidobenzyl radical (4OB•) and cluster-bound dehydroglycine (DHG) (Fig. 1B) (17). Electron and proton transfer to the 4OB• radical then yields the *p*-cresol product concomitant with the scission of DHG to form Fe-bound CO and CN^- and water (Fig. 1B). In this report, we explored the subsequent time course of the HydG reaction by using stopped-flow Fourier transform infrared (SF-FTIR) and electron-nuclear double resonance (ENDOR) spectroscopies to follow the synthesis of $Fe(CO)_x(CN)_y$ species and track them to the completion of the H-cluster bioassembly pathway.

SF-FTIR is a useful time-resolved method for studying the HydG reaction mechanism because CO and CN^- ligands give rise to strong infrared absorption bands with energies and intensities sensitive to the coordination and electronic environment of the bound Fe center. Figure 2 summarizes SF-FTIR data after the reaction of wild-type *Shewanella oneidensis* HydG ($HydG^{WT}$) with excess substrates SAM and ^{13}C-labeled Tyr [$(^{13}C)_9$-Tyr] in the presence of the reductant sodium dithionite (DTH). Observed bands are assigned to stretch vibrations of CO and CN ligands on the basis of their energy shifts upon ^{12}C:^{13}C and ^{14}N:^{15}N site-specific isotope substitution (fig. S2), which was achieved through use of the appropriate Tyr isotopologs (6). The time evolution of the resultant spectra (Fig. 2, A to C) reveals a stepwise conversion of a discrete intermediate, which we term complex A, to a distinct new species, complex B. Complex A is characterized by two bands at 1906 cm^{-1} and 2048 cm^{-1} [1949 cm^{-1} and 2093 cm^{-1} with ^{12}C-Tyr (Fig. 2D)], which we assign to stretching modes arising from terminal Fe-^{13}CO and Fe-^{13}CN moieties, respectively. The kinetic profile (Fig. 2B) shows that complex A accumulates on the same time scale as the decay of the previously observed 4OB• (17). Hence, the FTIR spectrum and formation kinetics of complex A are consistent with the mechanistic model in Fig. 1B, with the first turnover of HydG, SAM, and Tyr forming bound CO and CN^-, presumably on the unique

Fe site of the C-terminal 4Fe-4S cluster. Complex A does not form in the relatively conservative $Cys^{394} \rightarrow Ser^{394}$ (C394S), C397S HydG double mutant ($HydG^{SxxS}$), which lacks the C-terminal cluster (figs. S3 and S4).

Complex A reaches a maximum concentration and starts to decay after about 30 s, concomitant with the appearance and growth of complex B. The three bands associated with complex B have identical kinetics and may be assigned to terminal bound ligands: two high-energy, predominately $\nu(^{13}CO)$ modes at 1960 cm^{-1} and 2010 cm^{-1} and a $\nu(^{13}CN)$ mode at 2062 cm^{-1}. We assign the 2010 cm^{-1} band to a predominantly $\nu(^{13}CO)$ mode rather than a $\nu(^{13}CN)$ mode because its energy shifts upon ^{13}C isotopic substitution at the carboxyl position in Tyr [the moiety that gives rise to the CO but not the CN ligands in the mature H cluster (fig. S2)] (6). An additional band at 1906 cm^{-1} and shoulder at 2048 cm^{-1} likely arise from residual complex A.

A reasonable structure for complex B is a cuboidal $Fe(CO)_2(CN)$-[3Fe-4S] species in which the unique Fe site is coordinated by the three Tyr-derived diatomic ligands. For CO and CN^- ligands that are bound to a single Fe center, the $\nu(CO)$ and $\nu(CN)$ vibrational modes are expected to be strongly coupled. To test for vibrational mixing between the two observed $\nu(CO)$ frequencies, we generated a 1:2:1 mixture of $^{12}CO^{12}CO$-, $^{12}CO^{13}CO$-, and $^{13}CO^{13}CO$-labeled complex B from a 1:1 mixture of natural abundance Tyr and ^{13}COO-Tyr. If the two $\nu(CO)$ modes in complex B were not coupled, then the expected resulting spectrum would be a simple 1:1 superposition of the $^{12}CO^{12}CO$ and $^{13}CO^{13}CO$ spectra (Fig. 2E, lower trace). Instead, the observed spectrum displayed overlapping additional bands (Fig. 2E, upper trace) that can be ascribed to the two $^{12}CO^{13}CO$-labeled isotopomers with apparent CO-stretching frequencies shifted relative to their isotopically pure counterparts because of vibrational mixing of the two fundamental $\nu(CO)$ modes (fig. S6). Similarly, a comparison of spectra generated by using $(^{13}C)_9$-Tyr and $(^{13}C)_9$ ^{15}N-Tyr (Fig. 2F) shows that ^{15}N substitution produces both a smaller than expected energy shift in the $\nu(CN)$ mode as well as an energy shift in the higher energy $\nu(CO)$ mode, indicating that these modes are also vibrationally mixed. Taken together, these coupling data suggest that all three ligands (two CO and one CN^-) in complex B are bound to a single Fe-center.

The relatively high energies of the $\nu(CO)$ modes of complex B suggest that it may be appropriately modeled as a cationic, low-spin $[Fe(II)(CO)_2(CN)]^+$ complex based on comparisons with related neutral, low-spin $Fe(II)(CO)_2(CN)$ complexes (18, 19). The density functional theory (DFT)–calculated $\nu(CO)$ and $\nu(CN)$ frequencies and intensities of $[fac\text{-}(H_2S)_3Fe(II)(CO)_2(CN)]^+$, a simple model for $\{Fe(II)(CO)_2(CN)\text{-}[3Fe\text{-}4S]\}^+$, show reasonable agreement with the observed spectrum of complex B (fig. S5 and table S2). Alternative stereoisomers in which the CO and CN^- ligands are not cofacial or in which the sulfur donors are replaced with oxygen donors were not found to give rise to the expected intensity patterns. In addition, the coupling pattern in the $^{12}CO^{13}CO$ isotope mixture (Fig. 2E, top) was only reproduced computationally when the two CO ligands have different inherent $\nu(CO)$ energies, which could be explained by the electronic asymmetry of the coordinating $[3Fe\text{-}4S]^0$ subcluster (20) or by asymmetry in CO H-bonding interactions.

The kinetics in Fig. 2B suggest sequential conversion of complex A to complex B, which we associate with another turnover of HydG acting on a second substrate Tyr to form an additional CO to coordinate the unique Fe center of the C-terminal cluster (21). Unlike the first turnover (17), we have no experimental information at this time about how Tyr binds and what intermediates may be involved in this second reaction, although we note that our model for complex A is coordinatively unsaturated and could bind Tyr or a Tyr-derived fragment during the second turnover. Only at much longer times was free CO detected in solution through its binding to exogenous myoglobin (see green trace in Fig. 2B and fig. S3), which rules out the binding of externally derived CO as part of the mechanism. The release of free CO is correlated with the rise of complex A (Fig. 2B) at a late time (>300 s), suggesting that complex B may degrade to complex A by loss of CO when other H-cluster maturation components are not available to facilitate its incorporation into the proper downstream assembly products (vide infra). Reports of no lag phase in free CO production (12) may arise from alternative chemistry resulting from differences in experimental protocols.

To determine the fate of the Fe-containing complex B, we measured the continuous-wave (CW) EPR and pulse ENDOR spectra of HydA1 hydrogenase from *Chlamydomonas reinhardtii* that had been either uniformly or selectively labeled with ^{57}Fe [xxxxx (*I*) = 1 or 2]. Uniformly ^{57}Fe-labeled HydA1 (HydA1^{57Fe}) was generated by introducing ^{57}Fe into the growth media for HydA1. The *Q*-band Davies pulse ENDOR (22) spectrum of the purified HydA1^{57Fe} poised in the H_{ox} state is shown in Fig. 3A. This spectrum was obtained at the highest xxxxxx (*g*) value, $g_1 = 2.10$, where there is no overlap with the EPR signal from the CO-inhibited H_{ox}-CO form (fig. S7), and it shows several peaks in the 3- to 10-MHz range.

For a sample of HydA1 (that we term HydA1$^{57Fe–HydG}$) in which the $[2Fe]_H$ cluster was assembled in vitro (6, 7) by using HydE and HydF expressed in natural abundance media and HydG expressed in ^{57}Fe-enriched media (fig. S1), the ENDOR spectrum (Fig. 3B) was well simulated by a single doublet, with frequencies $\nu_{\pm} = A(^{57}Fe)/2 \pm \nu_I$, where $A(^{57}Fe)$ = 16.0 MHz is the effective hyperfine tensor component at this $g_1 = 2.10$ value and ν_I is the ^{57}Fe nuclear Zeeman frequency at this magnetic field. We assigned this doublet to the $[2Fe]_H$ subcluster, because the $[4Fe\text{-}4S]_H$ cluster is not labeled with ^{57}Fe for this sample. Subtraction of the ^{57}Fe ENDOR spectrum of the $[2Fe]_H$ subcluster–labeled sample from that of the HydA1^{57Fe} sample isolated the ^{57}Fe ENDOR signal that arose from the $[4Fe\text{-}4S]_H$ cluster (Fig. 3C), which was well simulated as an ENDOR doublet with $A(^{57}Fe)$ = 10.55 MHz. Both $A(^{57}Fe)$ values for HydA1 are consistent with previous ENDOR and Mössbauer spectroscopic studies of the H_{ox} state of *Desulfovibrio vulgaris* and *Clostridium pasteurianum* hydrogenases (≈16 to 18 MHz for the $[2Fe]_H$ subcluster and ≈ 8 to 10MHz for the $[4Fe\text{-}4S]_H$ cluster) (23–26), although they differ somewhat from those derived from ENDOR data for the *Desulfovibrio desulfuricans* hydrogenase (12.4 and 11.1 MHz, respectively) (*27*). Comparing the magnitudes of the two $A(^{57}Fe)$ values determined above confirms that the greatest spin density of the H-cluster in the H_{ox} state lies on the $[2Fe]_H$ subcluster. More importantly, these ENDOR data show that Fe in the $[2Fe]_H$ subcluster of the mature H-cluster originates from the HydG radical SAM maturase.

The SF-FTIR and ^{57}Fe ENDOR spectroscopic results presented in this report provide further insight into the assembly of the $[2Fe]_H$ subcluster of FeFe hydrogenase, illustrated in Fig. 4. Prior work demonstrated that the CO and CN^- ligands of the $[2Fe]_H$ subcluster are generated from Tyr via HydG. Results from SFFTIR spectroscopic studies provide evidence for the formation of two distinct Fe-bound CO and CN-containing species, complexes A and B, during the HydG reaction. Analysis of the vibrational mode coupling buttressed by DFT results on realistic model complexes lead us to postulate that complex B is a 3Fe-4S–bound $Fe(CO)_2(CN)$ species. The ^{57}Fe-labeling experiments prove that Fe in the $[2Fe]_H$ subcluster is provided by HydG. It is therefore straightforward to envisage a mechanism wherein two complex B units assemble together with a dithiolate bridge to form the $[2Fe]_H$ cluster. Our proposal for the structure of this deliverable species is consistent with all of the available data and points to the biologically relevant product of the HydG reaction as being an organometallic $Fe(CO)_2(CN)$ synthon.

Supplementary Material

Refer to Web version on PubMed Central for supplementary material.

Acknowledgments

This work was funded by the NIH (R.D.B., no GM072623; S.P.C., no. GM65440) and by the Division of Material Sciences and Engineering (J.R.S., award no. DE-FG02-09ER46632) of the Office of Basic Energy Sciences (OBER) of the U.S. Department of Energy (DOE), by DOE OBER (S.P.C.), and the UniCat Cluster of Excellence of the German Research Council (V.P.).

References and Notes

1. Vignais PM, Billoud B. Chem. Rev. 2007; 107:4206–4272. [PubMed: 17927159]
2. Vincent KA, Parkin A, Armstrong FA. Chem. Rev. 2007; 107:4366–4413. [PubMed: 17845060]
3. Adams MWW, Stiefel EI. Curr. Opin. Chem. Biol. 2000; 4:214–220. [PubMed: 10742193]
4. Shepard EM, et al. Proc. Natl. Acad. Sci. U.S.A. 2010; 107:10448–10453. [PubMed: 20498089]
5. Mulder DW, et al. Structure. 2011; 19:1038–1052. [PubMed: 21827941]
6. Kuchenreuther JM, George SJ, Grady-Smith CS, Cramer SP, Swartz JR. PLOS ONE. 2011; 6:e20346. [PubMed: 21673792]
7. Kuchenreuther JM, Britt RD, Swartz JR. PLOS ONE. 2012; 7:e45850. [PubMed: 23049878]
8. Berggren G, et al. Nature. 2013; 499:66–69. [PubMed: 23803769]
9. Esselborn J, et al. Nat. Chem. Biol. 2013; 9:607–609. [PubMed: 23934246]
10. Pilet E, et al. FEBS Lett. 2009; 583:506–511. [PubMed: 19166853]
11. Driesener RC, et al. Angew. Chem. Int. Ed. 2010; 49:1687–1690.
12. Shepard EM. J. Am. Chem. Soc. 2010; 132:9247–9249. [PubMed: 20565074]
13. Rubach JK, Brazzolotto X, Gaillard J, Fontecave M. FEBS Lett. 2005; 579:5055–5060. [PubMed: 16137685]
14. Tron C, et al. Eur. J. Inorg. Chem. 2011; 2011:1121–1127.
15. Frey PA, Hegeman AD, Ruzicka FJ. Crit. Rev. Biochem. Mol. Biol. 2008; 43:63–88. [PubMed: 18307109]
16. Vey JL, Drennan CL. Chem. Rev. 2011; 111:2487–2506. [PubMed: 21370834]
17. Kuchenreuther JM, et al. Science. 2013; 342:472–475. [PubMed: 24159045]
18. Piper TS, Cotton FA, Wilkinson G, Inorg J. Nucl. Chem. 1955; 1:165–174.
19. Darensbourg DJ. Inorg. Chem. 1972; 11:1606–1609.
20. Weigel JA, Holm RH, Surerus KK, Munck E. J. Am. Chem. Soc. 1989; 111:9246–9247.

21. This process would also entail formal loss of CN^-. Although the SF-FTIR data for complex B cannot rigorously exclude coordination by two CN^- groups, we consider this to be unlikely because only one n(CN) mode is observed and only one CN^- per Fe is present in both the assembled $[2Fe]_H$ subcluster and the synthetic dinuclear Fe compound that can activate the FeFe hydrogenase (8, 9)

22. Davies ER. Phys. Lett. A. 1974; 47:1–2.

23. Telser J, Benecky MJ, Adams MWW, Mortenson LE, Hoffman BM. J. Biol. Chem. 1986; 261:13536–13541. [PubMed: 3020036]

24. Telser J, Benecky MJ, Adams MWW, Mortenson LE, Hoffman BM. J. Biol. Chem. 1987; 262:6589–6594. [PubMed: 3032973]

25. Popescu CV, Munck E. J. Am. Chem. Soc. 1999; 121:7877–7884.

26. Pereira AS, Tavares P, Moura I, Moura JJG, Huynh BH. J. Am. Chem. Soc. 2001; 123:2771–2782. [PubMed: 11456963]

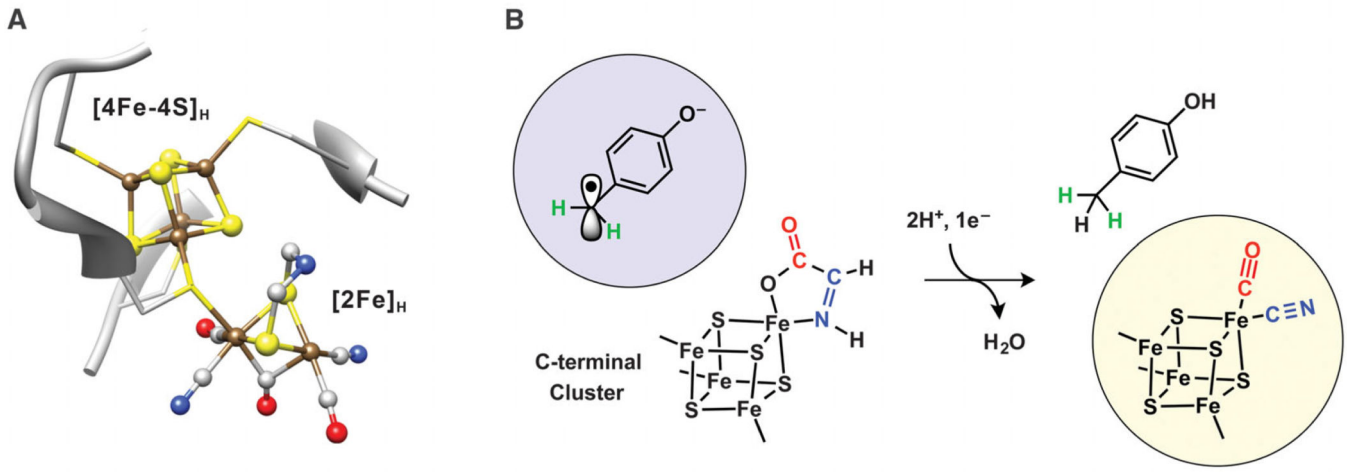

Fig. 1. Ligand synthesis by HydG

(**A**) The catalytic H-cluster of FeFe hydrogenases. Ball-and-stick representation (from Protein Data Bank entry 3C8Y) was generated by using University of California San Francisco Chimera: Fe (brown), S (yellow), C (gray), O (red), and N (blue). H was not shown for simplicity. (**B**) Proposed HydG-catalyzed conversion of 4Fe-4*S*–bound dehydroglycine to an Fe(CO)(CN) species concomitant with conversion of 4OB• to *p*-cresol (17).

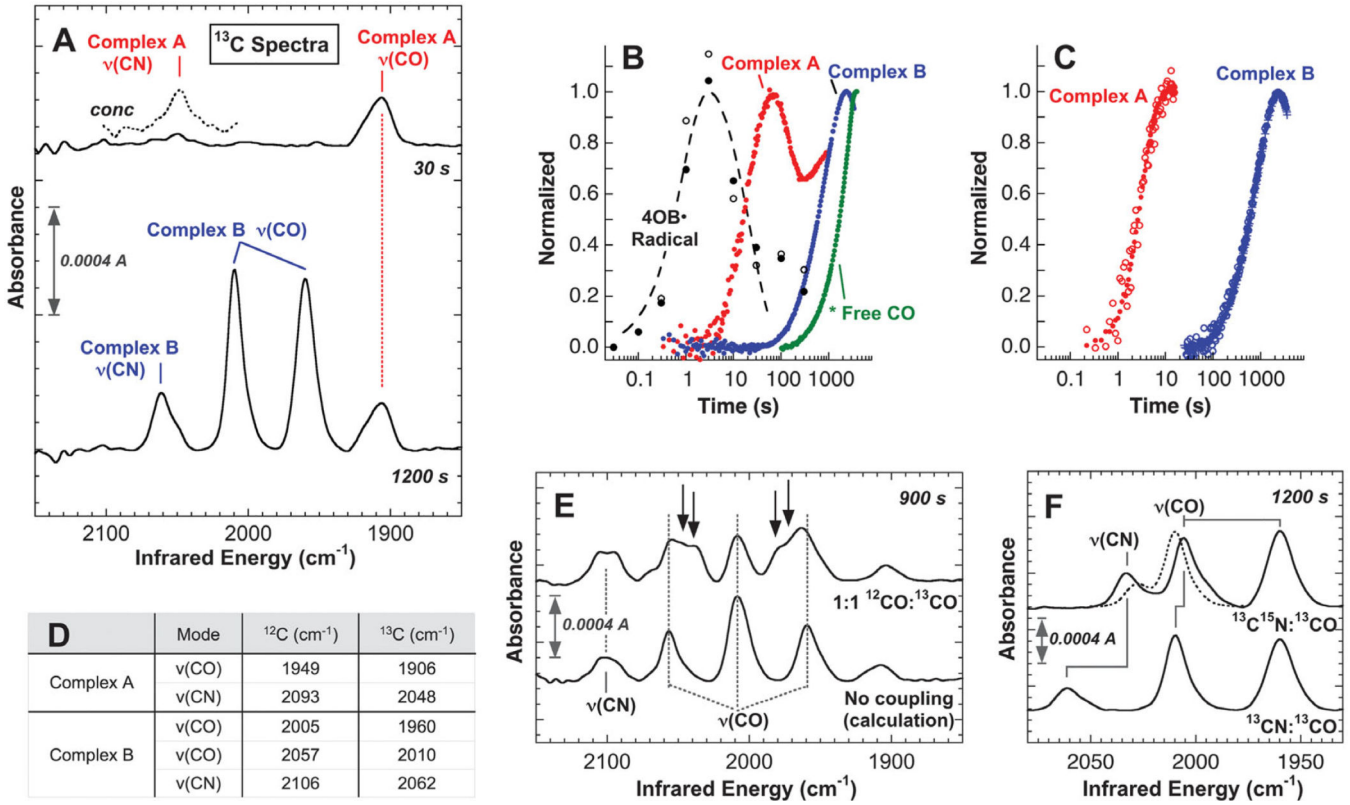

D	Mode	^{12}C (cm^{-1})	^{13}C (cm^{-1})
Complex A	ν(CO)	1949	1906
	ν(CN)	2093	2048
Complex B	ν(CO)	2005	1960
	ν(CO)	2057	2010
	ν(CN)	2106	2062

Fig. 2. FTIR spectra

Reactions used 100 μM HydG^{WT} and (^{13}C)$_9$-Tyr, producing ^{13}CO and ^{13}CN ligands, unless indicated otherwise. (**A**) SF-FTIR spectra measured at 30 and 1200 s (solid lines) and at 10 s using 800 μM HydG^{WT} (dotted line, plotted at half intensity). (**B**) Time dependence of formation and decay of the following species: 4OB• determined by EPR spectroscopy, two experimental runs (•, °) and corresponding kinetic fit (dashed line) (17); FTIR data (no kinetic fit) of complex A (red) and complex B (blue) determined by the peak heights of their respective ν(CO) modes [see (A)]; and free CO trapped by myoglobin (green) (fig. S3). Each data set is scaled to unity at its maximum value. (**C**) Comparison of the time dependence of the peak heights of all ν(CO) and ν(CN) bands for complex A and complex B. Complex A red symbols are as follows: °, ν(^{13}CN); •, ν(^{13}CO). Complex B blue symbols are as follows: °, ν(^{13}CN); •, ν(^{13}CO) 2010 cm^{-1}; +, ν(^{13}CO) 1960 cm^{-1}. The data for complex A were taken from measurements by using 800 μM HydG^{WT} in order to enhance the signal:noise ratio of the ν(CN) mode. (**D**) Table of frequencies for observed IR bands of complexes A and B prepared by using Tyr (middle column) or (^{13}C)$_9$-Tyr (right-most column). (**E**) SF-FTIR spectrum of complex B measured at 900 s and prepared by using a 1:1 mixture of Tyr and ^{13}COO-Tyr (top). Average of the ^{12}CO and ^{13}CO product B spectra (bottom). The arrows indicate new bands not present in either the ^{12}CO or ^{13}CO spectra of complex B. (**F**) SF-FTIR spectra of complex B measured at 1200 s and prepared by using (^{13}C)$_9$ ^{15N}-Tyr (top) and (^{13}C)$_9$Tyr (bottom). Expected (CN) and (CO) bands for ^{13}C^{15}N-containing complex B in the absence of ν(CN)/ ν(CO) vibrational mixing (dotted line). Predicted band shifts computed simply by the change in the reduced mass.

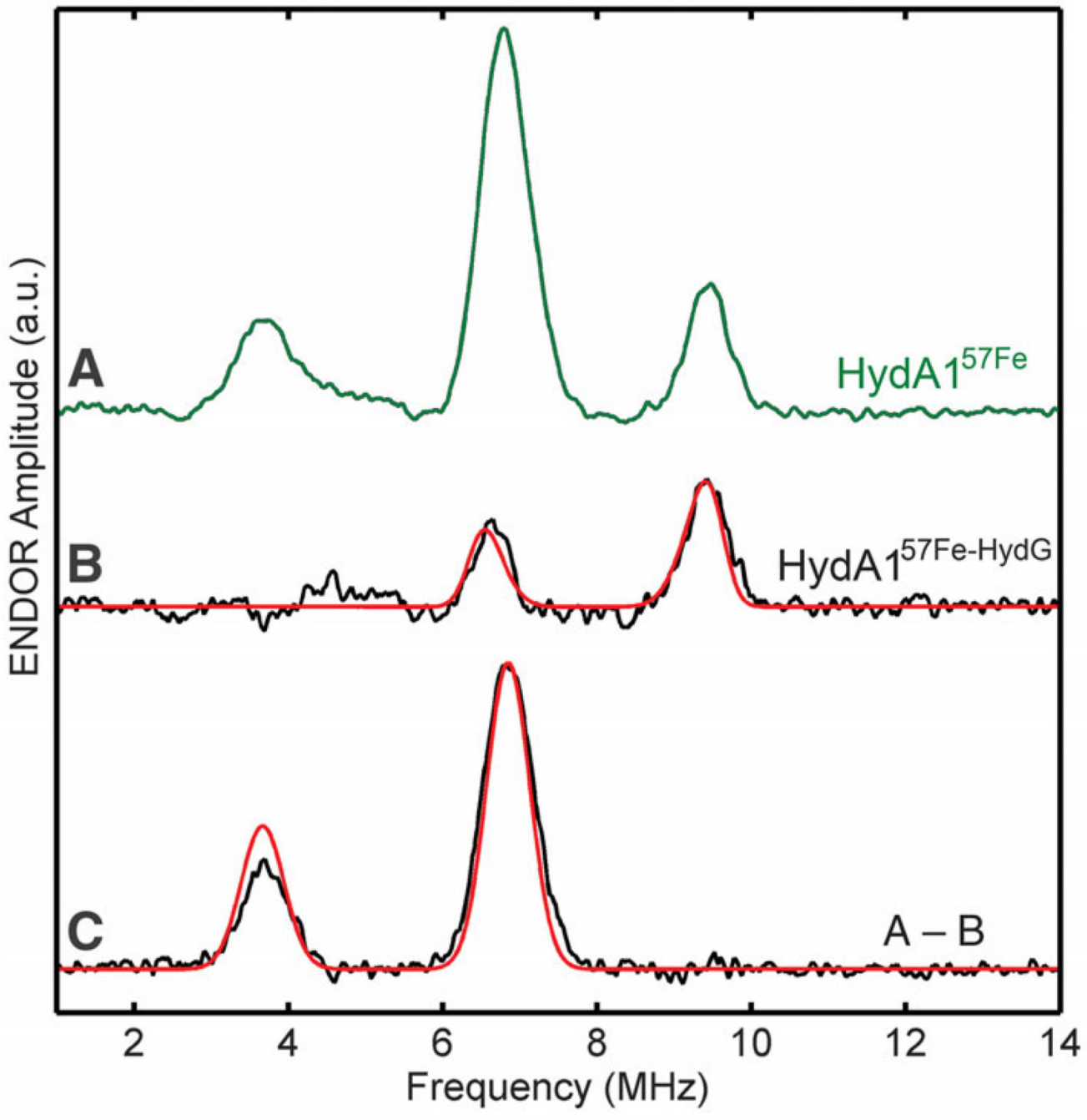

Fig. 3. *Q*-band (34.00 GHz, 1.155 T) Davies ENDOR spectra of FeFe hydrogenase HydA1 enriched with ^{57}Fe

(**A**) HydA1^{57Fe}; (**B**) HydA1$^{57Fe–HydG}$ [black, experiment; red, simulation with $A(^{57}Fe)$ = 16.0 MHz]; (**C**) (A) – (B) difference spectrum [black, experiment; red, simulation with $A(^{57}Fe)$ = 10.55 MHz]. ENDOR simulations used line widths of 0.4 and 0.65 MHz for $[2Fe]_H$ and $[4Fe\text{-}4S]_H$ components, respectively, with other values taken directly from experiment parameters and CW EPR simulations. The ENDOR spectrum of natural

abundance Fe HydA1 in the H_{ox} state was subtracted from both spectra (A) and (B). a.u., arbitrary units.

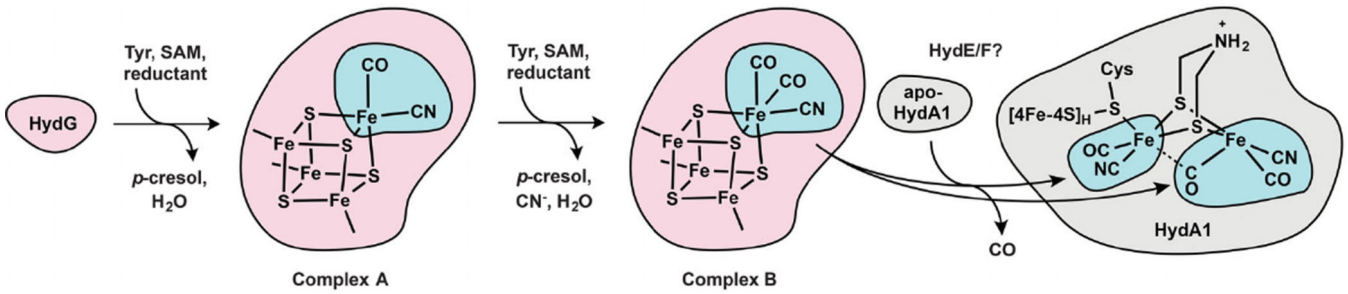

Fig. 4. Schematic for the bioassembly of the FeFe hydrogenase H-cluster via a HydG-synthesized $Fe(CO)_2(CN)$ synthon

Pink indicates xxxxx; cyan, xxxxx; gray, xxxxxxxx.